Proceedings of IMECE2007
2007 ASME International Mechanical Engineering Congress and Exposition
November 11-15, 2007, Seattle, Washington, USA

IMECE2007-42970

MODEL BASED CHARACTERIZATION OF TRANSIENT RESPONSE OF A SOLID OXIDE FUEL CELL SYSTEM

Tuhin Das *
Visiting Assistant Professor
Dept. of Mechanical Engineering
Michigan State University
East Lansing, Michigan 48824
Email: tuhindas@egr.msu.edu

Sridharan Narayanan
Graduate Student
Dept. of Mechanical Engineering
Michigan State University
East Lansing, Michigan 48824
Email: naraya22@egr.msu.edu

Ranjan Mukherjee
Professor
Dept. of Mechanical Engineering
Michigan State University
East Lansing, Michigan 48824
Email: mukherji@egr.msu.edu

ABSTRACT

In this paper we perform transient analysis of a Solid Oxide Fuel Cell (SOFC) system. We consider a steam reformer based SOFC system with anode recirculation and with methane as fuel. For the analysis, we develop a control-oriented model that captures the details of heat and mass transfer, chemical kinetics and electrochemistry of the SOFC system. The coupled dynamics of the steam reformer and the fuel cell anode control volumes are extracted and through coordinate transformations we derive closed-form expressions characterizing the steady-state and transient behaviors of two critical performance variables of reformer-based SOFC systems, namely utilization and steam-to-carbon balance. Our analysis is supported by simulations. Using the results derived, we address steady-state fuel optimization by posing it as a problem in linear programming. Our results can be applied in predicting system response to step changes in current and will be useful in designing control strategies for SOFC based power plants.

NOMENCLATURE

C_p	Specific heat at constant pressure (J/kg/K)
C_s	Specific heat of solid volume (J/kg/K)
C_v	Specific heat at constant volume (J/kg/K)
E_a, E_b, E_c	Activation energy of reactions (a), (b), (c) in Eqns.(6) and (17) (J/mol)
F	Faraday's constant ($=$ 96485.34 coulomb/mol)
h	Molar enthalpy (J/mole)
i	Current draw (amps)
k	Anode recirculation fraction
M_s	Mass of solid volume (kg)
MW	Molecular weight (kg/mol)
$\dot{M}_{in}$	Anode inlet mass flow rate (kg/sec)
$\dot{M}_o$	Anode exit mass flow rate (kg/sec)
N	Number of moles (moles)
N_c	Number of cells in series
$\dot{N}_{air}$	Molar flow rate of air (moles/sec)
$\dot{N}_f$	Molar flow rate of fuel (moles/sec)
$\dot{N}_{in}$	Anode inlet flow rate (moles/sec)
$\dot{N}_o$	Anode exit flow rate (moles/sec)
n	Number of electrons participating in electro-chemical reaction ($=2$)
P_g	Control volume pressure (N/m^2)
p	Partial pressure (N/m^2)
$\dot{Q}_g$	Rate of heat transfer to gas control volume (W)
$\dot{Q}_s$	Rate of heat transfer to solid volume (W)
R_u	Universal Gas Constant (8.314J/mol/K)
r_a, r_b, r_c	Rates of reactions (a), (b), (c) in Eqns.(6) and (17) (mol/kg cat./sec)
r_d	Rate of electro-chemical reaction (moles/sec)
$STCB$	Steam-To-Carbon Balance (moles/sec)
$STCR$	Steam-To-Carbon Ratio
T_g	Temperature of gas control volume (K)
T_{ref}	Reference temperature (K)
T_s	Temperature of solid volume (K)

*Address all correspondence to this author.

U	Utilization
V	Volume (m^3)
$\dot{W}_{net}$	Net work done (W)

Symbols

ΔH	Enthalpy of reaction or adsorption (J/mol)
Δh_f^o	Enthalpy of formation at 298K and 1atm (J/mol)
$\mathcal{K}_a$, $\mathcal{K}_c$	Equilibrium constant of reactions (a) and (c) in Eqns.(6) and (17) (Pa^2)
$\mathcal{K}_b$	Equilibrium constant of reactions (b) in Eqns.(6) and (17)
$\mathcal{K}_{CH_4}$, $\mathcal{K}_{CO}$, $\mathcal{K}_{H_2}$	Adsorption constant for CH_4, CO, H_2 (Pa^{-1})
$\mathcal{K}_{H_2O}$	Adsorption constant for H_2O
κ_a, κ_c	Rate coefficient of reaction (a) and (c) (mol $Pa^{0.5}$/kg cat/sec)
κ_b	Rate coefficient of reaction (b) (mol/kg cat/sec/Pa)
$\dot{\eta}$	Molar flow rate (moles/sec)
$\mathcal{R}$	Species rate of formation (moles/sec)
$\mathcal{X}$	Species mole fraction

Subscripts

a	Anode control volume
c	Cathode control volume
cv	Generic control volume
e	Exit condition of control volume
in	Inlet condition of control volume
i	Values of 1 through 7 represent CH_4, CO, CO_2, H_2, H_2O, N_2, and O_2
r	Reformate control volume
ss	Steady-state

INTRODUCTION

Research in the area of fuel cell systems has gathered significant momentum in recent years. Among the different fuel cell technologies, Solid Oxide Fuel Cell (SOFC) systems have attracted interest due to several factors. SOFC systems are solid state devices and are simpler in concept than other fuel cell technologies. Fuel flexibility and tolerance to impurities are attractive features of SOFCs. The high operating temperature (800 to 1000°C) are conducive to internal reforming of fuel to generate hydrogen rich gases. The exhaust gases are excellent means for sustaining on-board fuel reforming processes and tolerance to carbon monoxide simplifies the fuel reforming systems. Furthermore, SOFCs serve as excellent combined heat and power (CHP) systems. SOFC systems find applications typically in stationary power plants. High operating temperatures of SOFC systems contribute to thermal stresses, material failure and significant start-up times which have precluded their applications to automotive systems.

In this paper we perform model-based analysis of a steam reformer based tubular SOFC system with anode recirculation and methane as fuel. The system consists of three main components, a steam reformer, an SOFC, and a combustor. We develop a lumped control-oriented model that captures the details of heat and mass transfer, chemical kinetics and electro-chemical phenomena of the system. Our model has similarities with the tubular SOFC models developed in (1) and (2). The kinetics of steam reforming are modeled based on experimental results and observations in (3) and (4). Other tubular SOFC system models appear in (5), (6), (7) and (8), and models of planar SOFC systems appear in (9), (10), (11) and (12).

The transient response of a fuel cell system directly impacts its load following capability and determines the performance requirements on the power plants supplementary power source, such a battery or a super-capacitor. Hence, characterization of the transients of a fuel cell system will provide valuable insight towards design of the supplementary power source and in control development for the cumulative system. One of the earlier works on transient analysis of SOFC systems appears in (13) where the author applied dimensional analysis to characterize voltage transients due to load changes. Transient simulations of an SOFC-Gas Turbine hybrid system with anode recirculation is presented in (14). In (15), the authors simulate voltage response of a stand-alone SOFC plant to step changes in load and fuel and response to fast load variations. In (16), the authors study the detrimental effects of load transients due to differences in the response times of the SOFC, the power electronics, and the balance-of-plant components, and investigate the effectiveness of energy buffering devices such as a battery.

In this paper we derive closed form expressions that characterize the transient and steady-state behavior of fuel utilization and steam-to-carbon balance (STCB) of the SOFC system. To the best of our knowledge, such results have not appeared in the literature. Utilization is a critical variable in an SOFC system. High utilization implies high efficiency, however, too high a utilization leads to reduced partial pressure of hydrogen which can cause irreversible damages to the fuel cell due to anode oxidation (2). Typically 85% utilization is the target set for fuel cell control strategies. Steam-To-Carbon-Ratio (STCR) is another critical variable in steam-reformer based SOFC systems. STCR indicates the availability of steam for fuel reforming at the inlet of the reformer. A minimum STCR that allows stoichiometric combination of steam and carbon is necessary. For steam reforming of methane, a stoichiometric mixture has an STCR value of approximately 2. A mixture lean in steam causes catalyst deactivation through carbon deposition on the catalyst surfaces, (14), and hence must be prevented. In this paper, instead of STCR, we analyze the transient response of STCB due to its preferred mathematical form. Both utilization and STCR/STCB experience dramatic transients due to step changes in load and our study focuses on modeling these behaviors. This paper characterizes the faster

transients that arise from mass transfer and chemical kinetics. Temperature variation in SOFC systems occur at a significantly slower rate and simulations indicate that a quasi-steady thermal behavior can be assumed with minimal loss of accuracy.

This paper is organized as follows: In our discussion on SOFC model development, we first describe the SOFC system under consideration. In the subsequent section we develop the mathematical model of the SOFC system in three main subsections. We first present the equations for the fundamental gas and solid control volume models. The next subsections elaborate on the steam reformer and SOFC system models respectively where we focuss primarily on the mass transfer phenomena and chemical kinetics. Although not elaborated in our discussion, note that the heat transfer phenomena of the system is modeled in detail but omitted here for the sake of brevity. An open-loop simulation of the system model is provided next. Characterization of utilization and STCB/STCR are carried out and simulation results are provided in subsequent sections. Using results from prior sections, we next solve a steady-state fuel optimization problem. Finally, conluding remarks are provided followed by references.

SOFC MODEL DEVELOPMENT

SOFC System Description

In this section, we describe the steam reformer based tubular SOFC system which forms the basis of our analysis. The SOFC system is outlined in Fig.1. Methane is chosen as the fuel for the system, with a molar flow rate of $\dot{N}_f$. The reformer produces a hydrogen-rich gas which is supplied to the anode of the SOFC stack. Electrochemical reactions occuring at the anode due to current draw results in a steam-rich gas-mixture at the anode exit. A fraction k of the anode efflux is recirculated into the reformer through a mixing chamber where fuel is added. The mixing of the two fluid streams and pressurization is achieved using an ejector or a recirculating fuel pump, (14), (17). The steam reforming process occuring in the reformer catalyst bed is an endothermic process. The energy required to sustain the process is supplied from two sources, namely, the combustor efflux that is passed through the reformer, and the aforementioned recirculated flow which is also passed through the reformer before being injected into the mixing chamber, as shown in Fig.1. The remaining anode efflux is mixed with the cathode outflow in the combustion chamber. The combustor also serves to preheat the cathode air flow which has a molar flow rate of $\dot{N}_{air}$. The tubular construction of each cell causes the air to first enter the cell through the air supply tube and then reverse its direction to enter the cathode chamber. The cathode air serves as the source of oxygen for the fuel cell.

SOFC System Model

Fundamental Models The essential dynamics of the SOFC system in Fig.1 can be captured through the fundamental solid volume and gas control volume models.

Solid Volume Model: The thermodynamics of a solid volume can be expressed as

$$M_s C_s \dot{T}_s = \dot{Q}_s \tag{1}$$

Conductive heat transfers between solid control volumes is modeled using Fourier's Law and Newton's law is applied for modeling convective heat transfers between solid and gaseous control volumes, (2).

Gas Control Volume: The gas control volume model consists of energy and mass balance equations. Additonally, it captures the reaction kinetics arising from fuel reforming and electrochemistry. Throughout the model, gas composition and flow rate information are transmitted among control volumes using a uniform signal bus. Signals one through seven of the bus denote the seven relevant components, namely CH_4, CO, CO_2, H_2, H_2O, N_2, and O_2 respectively. The energy balance equation implemented for the generic gaseous control volume containing a gas mixture is

$$N_{cv} C_v \dot{T}_g = \dot{\eta}_{in} h_{in} - \dot{\eta}_e h_e + \dot{Q}_g - \dot{W}_{net} \tag{2}$$

The mass balance equation for individual species is constructed as follows,

$$N_{cv} \dot{\mathcal{X}}_{i,cv} = \dot{\eta}_{in} \mathcal{X}_{i,in} - \dot{\eta}_e \mathcal{X}_{i,cv} + \mathcal{R}_{i,cv}, \quad i = 1,2,\cdots,7 \tag{3}$$

where the subscripts i, $i = 1,2,\cdots,7$, correspond to the species CH_4, CO, CO_2, H_2, H_2O, N_2, and O_2 respectively. From Eqn.(3), we additionally have

$$\sum_{i=1}^{7} \mathcal{X}_{i,in} = \sum_{i=1}^{7} \mathcal{X}_{i,cv} = 1 \;\Rightarrow\; \sum_{i=1}^{7} \dot{\mathcal{X}}_{i,cv} = 0 \;\Rightarrow\; \dot{\eta}_e = \dot{\eta}_{in} + \sum_{i=1}^{7} \mathcal{R}_{i,cv} \tag{4}$$

From Eqns.(2) and (3) it is evident, that in our formulation the states of the gaseous control volume model are T_g and $\mathcal{X}_{i,cv}$, $i = 1,2,\cdots,7$. Flow is assumed to be governed by a nominal pressure drop across each module, (2), and hence is not treated as a state variable. The gas mixture is assumed to satisfy ideal gas laws and hence N_{cv} in Eqns.(2) and (3) is related to P_g and T_g through the equation $N_{cv} = P_g V_{cv} / R_u T_g$. In Eqn.(2), C_v, h_{in}, and h_e are related to the state variables through the following general

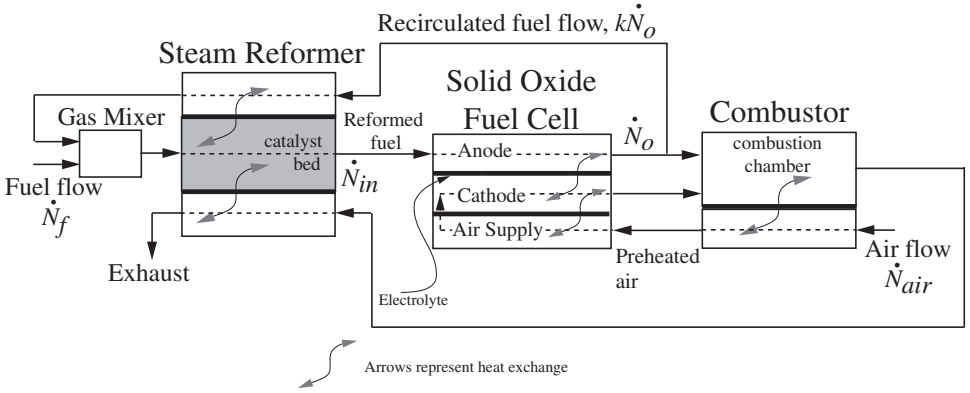

Figure 1. SCHEMATIC OF THE SOFC SYSTEM

equations:

$$\begin{aligned} C_v(T) &= \sum_{i=1}^{7} \mathcal{X}_i C_{p,i}(T) - R_u, \\ \tfrac{C_{p,i}(T)}{R_u} &= a_i + b_i T + c_i T^2 + d_i T^3 + e_i T^4, \\ h &= \sum_{i=1}^{7} \mathcal{X}_i \left(\int_{298}^{T} C_{p,i}(T)\, dT + \Delta h^o_{f,i} \right) \end{aligned} \tag{5}$$

$C_{p,i}$ is expressed in functional form using the coefficients a_i, b_i, c_i, d_i, e_i, as given in (18). The inlet enthalpy is computed using the gas inlet temperature T_{in} and that at the exit is computed using $T_e = T_g$.

Reformer Model For steam reforming of methane we consider a packed-bed tubular reformer with nickel-alumina catalyst, (19). A schematic diagram of the steam reformer is shown in Fig.2. The exhaust, steam and reformate flows are modeled

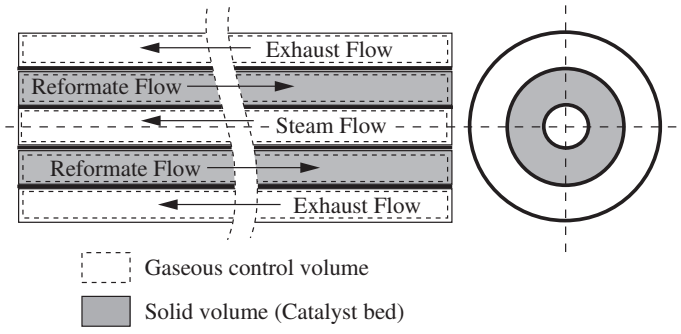

Figure 2. SCHEMATIC OF TUBULAR STEAM REFORMER

using gas control volumes and the catalyst bed is modeled as a solid volume. The details of the heat transfer characteristics of the system is given in (2) and is not repeated here. Instead, we emphasize on the reformer reaction kinetics and the mass transfer phenomena in light of the analyses presented in the following sections.

The three main reactions that simultaneously occur during steam reforming of methane, (1), (3), are:

$$\begin{aligned} &(a) \quad CH_4 + H_2O \leftrightarrow CO + 3H_2 \\ &(b) \quad CO + H_2O \leftrightarrow CO_2 + H_2 \\ &(c) \quad CH_4 + 2H_2O \leftrightarrow CO_2 + 4H_2 \end{aligned} \tag{6}$$

We use the following reaction rate expressions, given in (3), to model the reformer kinetics:

$$r_a = \frac{\kappa_a}{p_{H_2}^{2.5}} \left(p_{CH_4} p_{H_2O} - \frac{p_{H_2}^3 p_{CO}}{\mathcal{K}_a} \right) \Big/ \delta^2 \tag{7}$$

$$r_b = \frac{\kappa_b}{p_{H_2}} \left(p_{CO} p_{H_2O} - \frac{p_{H_2} p_{CO_2}}{\mathcal{K}_b} \right) \Big/ \delta^2 \tag{8}$$

$$r_c = \frac{\kappa_c}{p_{H_2}^{3.5}} \left(p_{CH_4} p_{H_2O}^2 - \frac{p_{H_2}^4 p_{CO_2}}{\mathcal{K}_c} \right) \Big/ \delta^2 \tag{9}$$

where

$$\begin{aligned} &\delta = 1 + \mathcal{K}_{CO} p_{CO} + \mathcal{K}_{H_2} p_{H_2} + \mathcal{K}_{CH_4} p_{CH_4} + \mathcal{K}_{H_2O} p_{H_2O} p_{H_2}, \\ &p_{\bar{q}} = \mathcal{X}_{\bar{q}} P,\ \bar{q} = CH_4, CO, CO_2, H_2, H_2O \end{aligned} \tag{10}$$

In Eqns.(7), (8) and (9), the rate coefficients κ_a, κ_b, and κ_c are given by

$$\kappa_j = \kappa_{j,T_{ref}} \exp\left[-\frac{E_j}{R_u} \left(\frac{1}{T} - \frac{1}{T_{ref}} \right) \right], \quad j = a, b, c, \tag{11}$$

and the adsorption constants $\mathcal{K}_{CO}$, $\mathcal{K}_{H_2}$, $\mathcal{K}_{CH_4}$, $\mathcal{K}_{H_2O}$ are expressed as follows

$$\mathcal{K}_q = \mathcal{K}_{q,T_{ref}} \exp\left[-\frac{\Delta H_q}{R_u}\left(\frac{1}{T}-\frac{1}{T_{ref}}\right)\right], q = CO, H_2, CH_4, H_2O \tag{12}$$

The values of T_{ref}, $\kappa_{j,T_{ref}}$, $\mathcal{K}_{q,T_{ref}}$, E_j and ΔH_q are given in (3). From the reforming reaction (a), (b) and (c) in Eqn.(6), we can express the rate of formation of individual species in the reformer in terms r_a, r_b and r_c, as follows

$$\begin{array}{ll} \mathcal{R}_{1,r} = -(r_a + r_c), & \mathcal{R}_{2,r} = (r_a - r_b), \\ \mathcal{R}_{3,r} = (r_b + r_c), & \mathcal{R}_{4,r} = (3r_a + r_b + 4r_c), \\ \mathcal{R}_{5,r} = -(r_a + r_b + 2r_c), & \mathcal{R}_{6,r} = 0, \\ \mathcal{R}_{7,r} = 0 & \end{array} \tag{13}$$

where r_a, r_b and r_c are computed using reformer temperature T_r, pressure P_r, mole fractions $\mathcal{X}_{\bar{q},r}$ and the total catalyst mass in the packed bed reformer. In Eqn.(13), any two of $\mathcal{R}_{1,r}$, $\mathcal{R}_{2,r}$, $\mathcal{R}_{3,r}$, $\mathcal{R}_{4,r}$ and $\mathcal{R}_{5,r}$ are independent. In general, for the reforming reactions in Eqn.(6), it can be shown that the rates of formation of any two of CH_4, CO, CO_2, H_2 and H_2O determine the rate of formation of the rest. Considering the rate of formation of CH_4 and CO in the reformer to be independent variables, we can write

$$\mathcal{R}_{3,r} = -\mathcal{R}_{1,r} - \mathcal{R}_{2,r},\ \mathcal{R}_{4,r} = -4\mathcal{R}_{1,r} - \mathcal{R}_{2,r},\ \mathcal{R}_{5,r} = 2\mathcal{R}_{1,r} + \mathcal{R}_{2,r} \tag{14}$$

Referring to Fig.1 and from Eqns.(3) and (14), the mass balance equations for CH_4, CO, CO_2, H_2 and H_2O can be written as follows:

$$\begin{array}{l} N_r \dot{\mathcal{X}}_{1,r} = k\dot{N}_o \mathcal{X}_{1,a} - \dot{N}_{in}\mathcal{X}_{1,r} + \mathcal{R}_{1,r} + \dot{N}_f \\ N_r \dot{\mathcal{X}}_{2,r} = k\dot{N}_o \mathcal{X}_{2,a} - \dot{N}_{in}\mathcal{X}_{2,r} + \mathcal{R}_{2,r} \\ N_r \dot{\mathcal{X}}_{3,r} = k\dot{N}_o \mathcal{X}_{3,a} - \dot{N}_{in}\mathcal{X}_{3,r} - \mathcal{R}_{1,r} - \mathcal{R}_{2,r} \\ N_r \dot{\mathcal{X}}_{4,r} = k\dot{N}_o \mathcal{X}_{4,a} - \dot{N}_{in}\mathcal{X}_{4,r} - 4\mathcal{R}_{1,r} - \mathcal{R}_{2,r} \\ N_r \dot{\mathcal{X}}_{5,r} = k\dot{N}_o \mathcal{X}_{5,a} - \dot{N}_{in}\mathcal{X}_{5,r} + 2\mathcal{R}_{1,r} + \mathcal{R}_{2,r} \end{array} \tag{15}$$

with $N_r = P_r V_r / R_u T_r$. Note that the reformer inlet and exit flows, as shown in Fig.1, do not contain O_2 and N_2. As a result, $\mathcal{X}_{6,r} = \mathcal{X}_{7,r} = 0$ and hence we disregard the mass balance equations of N_2 and O_2 corresponding to $i = 6$ and 7 respectively. From Eqns.(4) and (15) we deduce that

$$\dot{N}_{in} = k\dot{N}_o + \dot{N}_f + \sum_{i=1}^{7} \mathcal{R}_{i,r} \quad \Rightarrow \quad \dot{N}_{in} = k\dot{N}_o + \dot{N}_f - 2\mathcal{R}_{1,r} \tag{16}$$

SOFC Model Tubular Solid Oxide Fuel Cells are considered for our system analysis. A schematic diagram of an SOFC is shown in Fig.3. The anode, cathode and feed air flows are modeled using gas control volumes. The air feed tube and the electrolyte are modeled as solid volumes. Details of the heat transfer characteristics of these control volumes and voltage computations are given in (2) and is not repeated here. Instead, we emphasize on the fuel cell chemical kinetics and mass transfer phenomena as in the previous section.

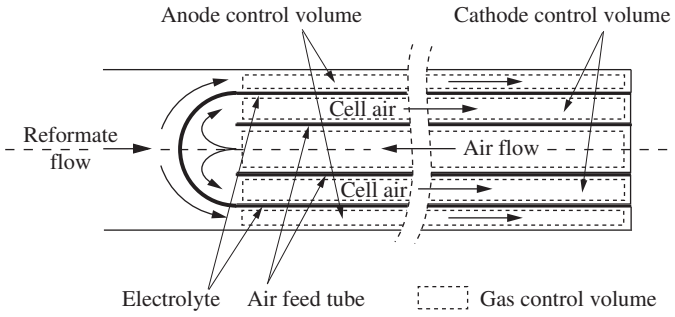

Figure 3. SCHEMATIC DIAGRAM OF TUBULAR SOFC

Anode control volume: The following chemical and electrochemical reactions are considered to occur simultaneously in the anode control volume:

$$\begin{array}{ll} (a) & CH_4 + H_2O \leftrightarrow CO + 3H_2 \\ (b) & CO + H_2O \leftrightarrow CO_2 + H_2 \\ (c) & CH_4 + 2H_2O \leftrightarrow CO_2 + 4H_2 \\ (d) & H_2 + O^{2-} \rightarrow H_2O + 2e \end{array} \tag{17}$$

The occurance of the reactions (a), (b) and (c) are due to internal reforming in the anode control volume which is aided by the elevated cell temperatures in SOFC and due to the presence of nickel catalyst in the anode. Electrochemical conversion of CO to CO_2 at the anode is also possible in parallel to the electrochemical process of steam generation from H_2. However, as pointed out in (20) and references therein, this reaction is much slower in presence of reactions (b) and (d) in Eqn.(17) and is therefore ignored in our analysis.

The rate of internal reforming reactions in the anode control volume, namely (a), (b) and (c), are modeled as given in Eqn.(9). The rate coefficients κ_j and the adsorption constants $\mathcal{K}_q$ in Eqns.(11) and (12) are calculated with T_a instead of T_g. The rate of electrochemical reaction (d) is given as the following function of current draw

$$r_d = \frac{iN_c}{nF} \tag{18}$$

The rates of formation of the individual gas species in the anode

control volume are expressed as follows

$$\begin{array}{ll} \mathcal{R}_{1,a} = -(r_a + r_c), & \mathcal{R}_{2,a} = (r_a - r_b), \\ \mathcal{R}_{3,a} = (r_b + r_c), & \mathcal{R}_{4,a} = (3r_a + r_b + 4r_c) - r_d, \\ \mathcal{R}_{5,a} = -(r_a + r_b + 2r_c) + r_d, & \mathcal{R}_{6,a} = 0, \\ \mathcal{R}_{7,a} = 0 & \end{array} \tag{19}$$

For the fuel cell, r_a, r_b and r_c are computed using Eqns.(7), (8), (9), (10), (11), (12), with anode temperature T_a, pressure P_a, mole fractions $\mathcal{X}_{\bar{q},a}$ and using the total anode catalyst mass. As shown in Eqn.(14), with $\mathcal{R}_{1,a}$, $\mathcal{R}_{2,a}$ and r_d as independent variables, we similarly have

$$\begin{array}{l} \mathcal{R}_{3,a} = -\mathcal{R}_{1,r} - \mathcal{R}_{2,r}, \\ \mathcal{R}_{4,a} = -4\mathcal{R}_{1,r} - \mathcal{R}_{2,r} - r_d, \\ \mathcal{R}_{5,a} = 2\mathcal{R}_{1,r} + \mathcal{R}_{2,r} + r_d \end{array} \tag{20}$$

Referring to Fig.1 and from Eqns.(3) and (20), the mass balance equations for CH_4, CO, CO_2, H_2 and H_2O in the anode control volume can be written as follows:

$$\begin{array}{l} N_a \dot{\mathcal{X}}_{1,a} = -\dot{N}_o \mathcal{X}_{1,a} + \dot{N}_{in} \mathcal{X}_{1,r} + \mathcal{R}_{1,a} \\ N_a \dot{\mathcal{X}}_{2,a} = -\dot{N}_o \mathcal{X}_{2,a} + \dot{N}_{in} \mathcal{X}_{2,r} + \mathcal{R}_{2,a} \\ N_a \dot{\mathcal{X}}_{3,a} = -\dot{N}_o \mathcal{X}_{3,a} + \dot{N}_{in} \mathcal{X}_{3,r} - \mathcal{R}_{1,a} - \mathcal{R}_{2,a} \\ N_a \dot{\mathcal{X}}_{4,a} = -\dot{N}_o \mathcal{X}_{4,a} + \dot{N}_{in} \mathcal{X}_{4,r} - 4\mathcal{R}_{1,a} - \mathcal{R}_{2,a} - r_d \\ N_a \dot{\mathcal{X}}_{5,a} = -\dot{N}_o \mathcal{X}_{5,a} + \dot{N}_{in} \mathcal{X}_{5,r} + 2\mathcal{R}_{1,a} + \mathcal{R}_{2,a} + r_d \end{array} \tag{21}$$

with $N_a = P_a V_a / R_u T_a$. As with the reformate control volume, the anode inlet and exit flows, do not contain O_2 and N_2. Therefore, $\mathcal{X}_{6,r} = \mathcal{X}_{7,r} = 0$, and hence we disregard the mass balance equations of N_2 and O_2. From Eqns.(4) and (21) we deduce that

$$\dot{N}_o = \dot{N}_{in} + \sum_{i=1}^{7} \mathcal{R}_{i,a} \quad \Rightarrow \quad \dot{N}_o = \dot{N}_{in} - 2\mathcal{R}_{1,a} \tag{22}$$

Cathode control volume: The electro-chemical conversion of O_2 to O^{2-} ions takes place in the cathode control volume.

$$\frac{1}{2} O_2 + 2e \rightarrow O^{2-} \tag{23}$$

with the reaction rate as given in Eqn.(18). Considering the mole fractions of N_2 and O_2 in air to be 0.79 and 0.21 respectively, the mass balance equations of the cathode control volume can be written from Eqns.(18) and (23) as follows:

$$\begin{array}{l} N_c \dot{\mathcal{X}}_{6,c} = 0.79\dot{N}_{air} - \left(\dot{N}_{air} - \frac{r_d}{2}\right) \mathcal{X}_{6,c} \\ N_c \dot{\mathcal{X}}_{7,c} = 0.21\dot{N}_{air} - \left(\dot{N}_{air} - \frac{r_d}{2}\right) \mathcal{X}_{7,c} - \frac{r_d}{2} \\ \mathcal{X}_{i,c} = 0, \quad i = 1, 2, \cdots, 5 \end{array} \tag{24}$$

Combustor Model The combustion reactions in the combustion chamber is assumed to achieve 100% oxidation of fuel. The combustor is modeled with three control volumes, namely, the combustion chamber, the air control volume, and the separator solid control volume. For conciseness, the details of the combustor model are omitted here.

Simulations

In this section we provide results of open-loop simulation of the SOFC system model. We consider a system with 100 cells in series, a fuel (pure CH_4) flow of 0.0034 moles/sec, air flow of 0.035 moles/sec, and a recirculation of 69%. The simulation results are shown in Fig.4. The load current is changed in steps as shown in Fig.4(a). The cell voltage and temperature changes corresponding to the changes in the current are shown Figs.4(b) and (d). Figs.4(e) and (f) depict the mole fractions of the species at reformer exit and anode exit respectively. The H_2O concentration is higher and the H_2 concentration is lower at the anode exit in comparison to the reformer exit. This is an expected outcome of current draw. The near equilibrium condition of the Water-Gas-Shift reaction in the anode (reaction (c) of Eqn.(17)) is evident through the sharp depletion of CO correponding to the depletion of H_2 due to current draw, as shown in Fig.4(f), especially around 500s to 700s when the current demand was maximum. Internal reforming in the anode control volume is illustrated by the negligible concentration of CH_4 at the anode exit in Fig.4(f).

In Fig.4(c), utilization and steam-to-carbon ratio are depicted. As mention in the introduction, utilization and Steam-To-Carbon-Ratio (STCR) are critical variables of an SOFC system. For the steam-reformer based SOFC system in consideration, the former is defined as the difference in the H_2 availability between the inlet and exit flows of the anode over the net H_2 availability at the anode inlet. The later is defined as the ratio of concentration of steam molecules to that of carbon atoms in the inlet of the reformer.

CHARACTERIZATION OF UTILIZATION

Steady-state and Transient Characteristics

To gain understanding of the dynamics of utilization, we perform an analysis based on the state-space models derived in previous sections. Based on the state variable definitions in Eqns.(15) and (21), fuel utilization can be written as follows:

$$U = 1 - \frac{\dot{N}_o \left(4\mathcal{X}_{1,a} + \mathcal{X}_{2,a} + \mathcal{X}_{4,a}\right)}{\dot{N}_{in} \left(4\mathcal{X}_{1,r} + \mathcal{X}_{2,r} + \mathcal{X}_{4,r}\right)} \tag{25}$$

Eqn.(25) is based on the internal reforming capability of the fuel cell anode where a CH_4 and a CO molecule can yield four and one molecules of H_2 respectively, as indicated by reaction (a), (b) and (c) in Eqn.(17). We rewrite Eqn.(25) with the coordinate

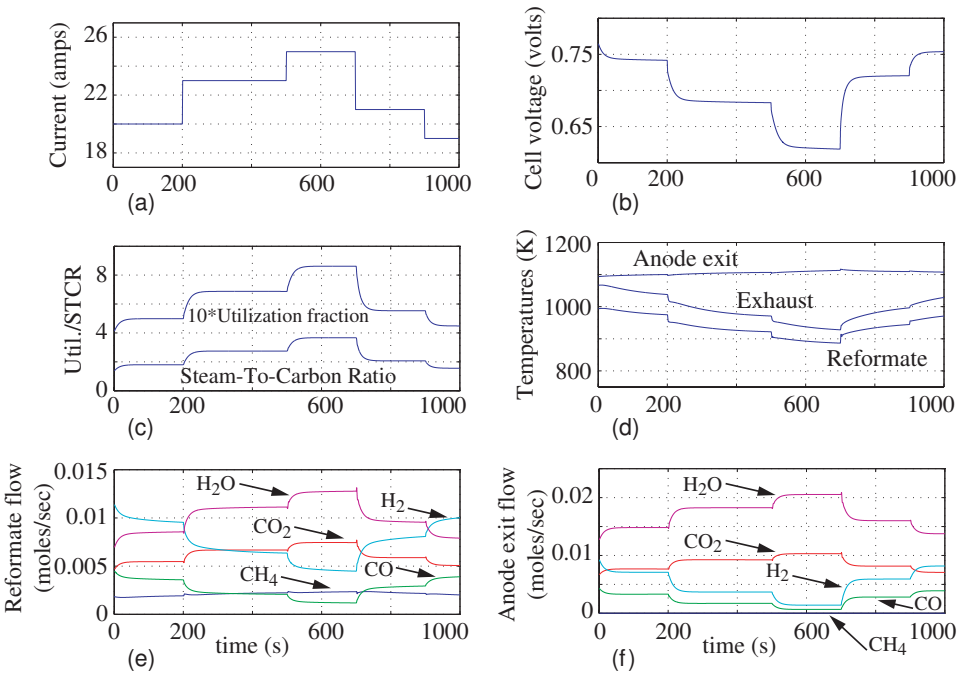

Figure 4. OPEN-LOOP SIMULATION OF STEAM REFORMER BASED SOFC SYSTEM

transformations as shown below:

$$U = 1 - \frac{\dot{N}_o \zeta_a}{\dot{N}_{in} \zeta_r}, \quad \begin{array}{l} \zeta_r = 4\mathcal{X}_{1,r} + \mathcal{X}_{2,r} + \mathcal{X}_{4,r} \\ \zeta_a = 4\mathcal{X}_{1,a} + \mathcal{X}_{2,a} + \mathcal{X}_{4,a} \end{array} \tag{26}$$

Using Eqns.(26), (15) and (21) the following state variable descriptions for ζ_r and ζ_a can be obtained:

$$\dot{\mathbf{Z}} = \mathbf{A}_1 \mathbf{Z} + \mathbf{B}_1, \mathbf{Z} = \begin{bmatrix} \zeta_r \\ \zeta_a \end{bmatrix}, \mathbf{A}_1 = \begin{bmatrix} -\frac{\dot{N}_{in}}{N_r} & \frac{k\dot{N}_o}{N_r} \\ \frac{\dot{N}_{in}}{N_a} & -\frac{\dot{N}_o}{N_a} \end{bmatrix}, \mathbf{B}_1 = \begin{bmatrix} \frac{4\dot{N}_f}{N_r} \\ \frac{-i\dot{N}_c}{nFN_a} \end{bmatrix} \tag{27}$$

It is interesting to note here that Eqn.(27) is devoid of the reaction rates $\mathcal{R}_{1,r}$, $\mathcal{R}_{2,r}$, $\mathcal{R}_{1,a}$, and $\mathcal{R}_{2,a}$. This removes the nonlinearities associated with the reaction rates as given in Eqns.(7) through (13) and Eqn.(19). Nevertheless, $\dot{N}_{in}$, $\dot{N}_o$, N_r, N_a are nonlinear functions of the states, temperatures and pressures given by

$$\dot{N}_{in} = \frac{\dot{M}_{in}}{\sum_{i=1}^{5} \mathcal{X}_{i,r} MW_i}, \dot{N}_o = \frac{\dot{M}_o}{\sum_{i=1}^{5} \mathcal{X}_{i,a} MW_i}, N_r = \frac{P_r V_r}{R_u T_r}, N_a = \frac{P_a V_a}{R_u T_a} \tag{28}$$

From Eqn.(27), we obtain the following expression relating U, k, i and $\dot{N}_f$ at steady-state

$$U_{ss} = \frac{1-k}{\frac{4nF\dot{N}_f}{i\dot{N}_c} - k} \tag{29}$$

Eqn.(29) is independent of the nonlinear variables given in Eqn.(28). Furthermore, since k, i and $\dot{N}_f$ are measurable and known quantities, Eqn.(29) can be used to exactly predict the steady-state fuel utilization for any given set of inputs.

From Eqns.(26) and (27) we note that the transient behavior of U can be predicted from the transient response of ζ_r, ζ_a, $\dot{N}_o$ and $\dot{N}_{in}$. We specifically consider the transient response of U due to step changes in i, when k and $\dot{N}_f$ are constant. In predicting the transient characteristics we assume that, in the process of a step change in i, the variables $\dot{N}_{in}$ and $\dot{N}_o$ can be treated as constants without significant loss of accuracy. With this assumption, Eqn.(27) reduces to a Linear Time Invariant (LTI) system with eigenvalues of $\mathbf{A}_1$ as:

$$\begin{aligned} \lambda_{1,2} &= 0.5\left[-\left(\frac{\dot{N}_{in}}{N_r} + \frac{\dot{N}_o}{N_a}\right) \pm \left(\left|\frac{\dot{N}_{in}}{N_r} - \frac{\dot{N}_o}{N_a}\right| + \alpha\right)\right], \\ \alpha &= \left[\left(\frac{\dot{N}_{in}}{N_r} - \frac{\dot{N}_o}{N_a}\right)^2 + 4k\frac{\dot{N}_{in}}{N_r}\frac{\dot{N}_o}{N_a}\right]^{1/2} - \left|\frac{\dot{N}_{in}}{N_r} - \frac{\dot{N}_o}{N_a}\right|, \quad \alpha \geq 0 \end{aligned} \tag{30}$$

Since $k \in (0,1)$, the eigenvalues of $\mathbf{A}_1$ are real and negative. The time constant for ζ_r, ζ_a, and hence that for U due to a step change in i will be determined by the maximum eigenvalue of $\mathbf{A}_1$. From Eqn.(30),

$$\begin{array}{l} \frac{\dot{N}_{in}}{N_r} \geq \frac{\dot{N}_o}{N_a} \rightarrow \lambda_{max} = -\frac{\dot{N}_o}{N_a} + 0.5\alpha \\ \frac{\dot{N}_{in}}{N_r} < \frac{\dot{N}_o}{N_a} \rightarrow \lambda_{max} = -\frac{\dot{N}_{in}}{N_r} + 0.5\alpha \end{array} \tag{31}$$

Simulations

In this section we provide simulation results in support of our analysis in the previous section. We run multiple simulations of the SOFC system with step changes in current applied at $t =$ 50s, as shown in Fig.5. The step changes in current are from

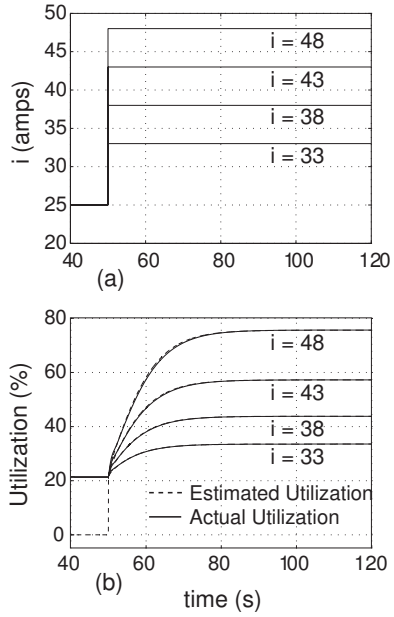

Figure 5. TRANSIENT AND STEADY-STATE UTILIZATION

25A to 33, 38, 43 and 48A as shown in Fig.5(a). For all four simulations, the following settings were used

$$\dot{N}_f = 0.0068\,\text{moles/s}, \quad \dot{N}_{air} = 0.0692\,\text{moles/s}, \quad k = 70\%.$$

In Fig.5(b) the transient response of utilization is plotted for the four simulations. The estimated utilization are obtained by simulating Eqns.(26) and (27) as an LTI system with $\mathbf{A}_1$ evaluated at the instant $t = 50$s. The following values were observed at $t = 50$s

$$\begin{array}{l} \dot{N}_{in} = 0.0624\,\text{moles/s} \\ \dot{N}_o = 0.0681\,\text{moles/s} \\ N_r = 0.0263\,\text{mole} \\ N_a = 0.1105\,\text{mole} \end{array} \quad \Rightarrow \quad \begin{array}{l} \lambda_1 = -2.8347 \\ \lambda_2 = -0.1543 \end{array}$$

Both the transient response as well as the steady-state value of estimated utilization match very closely with the non-linear model based calculation, as shown in Fig.5(b). The settling time computed based on 2% error is $T_s = 4/|\lambda_2| = 25.9235$s which matches well with the simulations.

CHARACTERIZATION OF STEAM-TO-CARBON BALANCE

Steady-state and Transient Characteristics

The Steam-To-Carbon-Ratio (STCR) is defined for the inlet flow of the steam reformer and can be mathematically expressed using Fig.1 as

$$\text{STCR} = \frac{k\dot{N}_o \mathcal{X}_{5,a}}{\dot{N}_f + k\dot{N}_o \mathcal{X}_{1,a} + k\dot{N}_o \mathcal{X}_{2,a}} \tag{32}$$

As the name suggests and is indicated by Eqn.(32), STCR is the ratio of the concentration of steam molecules to that of carbon atoms at the inlet of the reformer. The reactions (b) and (c) of Eqn.(6) indicate that the stoichiometric quantity of steam required for reforming is two moles and one mole of steam for each mole of CH_4 and CO respectively. With this understanding, we define a new variable, namely the Steam-To-Carbon-Balance (STCB), which is mathematically expressed as

$$\begin{aligned} \text{STCB} &= k\dot{N}_o \mathcal{X}_{5,a} - \left(2\dot{N}_f + 2k\dot{N}_o \mathcal{X}_{1,a} + k\dot{N}_o \mathcal{X}_{2,a}\right) \\ &= k\dot{N}_o \left(\mathcal{X}_{5,a} - 2\mathcal{X}_{1,a} - \mathcal{X}_{2,a}\right) - 2\dot{N}_f \end{aligned} \tag{33}$$

A positive value of STCB is an indication of sufficient steam at the reformer inlet for steam reforming and hence it is an indication of a favorable STCR. We rewrite Eqn.(33) with the coordinate transformations as shown below:

$$\text{STCB} = k\dot{N}_o \xi_a - 2\dot{N}_f, \quad \begin{array}{l} \xi_r = \mathcal{X}_{5,r} - 2\mathcal{X}_{1,r} - \mathcal{X}_{2,r} \\ \xi_a = \mathcal{X}_{5,a} - 2\mathcal{X}_{1,a} - \mathcal{X}_{2,a} \end{array} \tag{34}$$

Using Eqns.(34), (15) and (21) the state variable descriptions for ξ_r and ξ_a can be written as

$$\dot{\mathbf{S}} = \mathbf{A}_2\mathbf{S} + \mathbf{B}_2,\ \mathbf{S} = \begin{bmatrix} \xi_r \\ \xi_a \end{bmatrix},\ \mathbf{A}_2 = \begin{bmatrix} -\frac{\dot{N}_{in}}{N_r} & \frac{k\dot{N}_o}{N_r} \\ \frac{\dot{N}_{in}}{N_a} & -\frac{\dot{N}_o}{N_a} \end{bmatrix},\ \mathbf{B}_2 = \begin{bmatrix} \frac{-2\dot{N}_f}{N_r} \\ \frac{i\dot{N}_c}{nFN_a} \end{bmatrix} \tag{35}$$

Note that, as in Eqn.(27), the variables ξ_r and ξ_a in Eqn.(35) are independent of $\mathcal{R}_{1,r}$, $\mathcal{R}_{2,r}$, $\mathcal{R}_{1,a}$, and $\mathcal{R}_{2,a}$. $\dot{N}_{in}$, $\dot{N}_o$, N_r, N_a are nonlinear functions of the states, temperatures and pressures given by Eqn.(28). From Eqn.(35), the following steady-state expression for STCB is obtained

$$\text{STCB}_{ss} = \frac{1}{k-1}\left(2\dot{N}_f - \frac{kiN_c}{nF}\right) \tag{36}$$

Note, from Eqns.(27) and (35), that $\mathbf{A}_2 = \mathbf{A}_1$. Hence, the time constant in the transient response of STCB due to step changes in the current demand can be estimated using the eigenvalues $\lambda_{1,2}$ of $\mathbf{A}_1$ given in Eqn.(30). The discussion around Eqns.(30) and (31) is also applicable for transient response of STCB.

Simulations

The simulation results provided here are continuation of those provided above for step response of utilization in Figs.5(a) and (b). In Figs.6(a) and (b), STCR and STCB are plotted for the four simulations described in Fig.5(a). In Fig.6(b) the transient

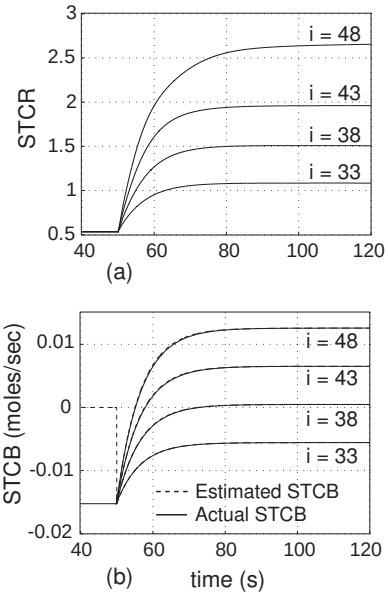

Figure 6. TRANSIENT AND STEADY-STATE STCR AND STCB

response of STCB are plotted. The estimated STCB are computed by considering the system given in Eqns.(34) and (35) as an LTI system with $\mathbf{A}_2$ evaluated at the instant $t = 50$s. Both the transient response as well as the steady-state value of estimated STCB match very closely with the non-linear model based calculation, as shown in Fig.6(b).

STEADY-STATE FUEL OPTIMIZATION

Problem Statement

Using the above derived results, we address a steady-state constrained fuel optimization problem which is stated as follows: Given that utilization and anode recirculation must be constrained within ranges $U_{ss} \in [U_{ss1}, U_{ss2}]$, $0 < U_{ss1}, U_{ss2} < 1$ and $k \in [k_a, k_b]$, $0 < k_a, k_b < 1$ respectively, and given a current i

1. Determine condition(s) under which there exists a range of solutions for $\dot{N}_f$ that satisfies the constraints above and maintains STCB ≥ 0.
2. If a range of solutions exists, determine the minimum fuel operating conditions.

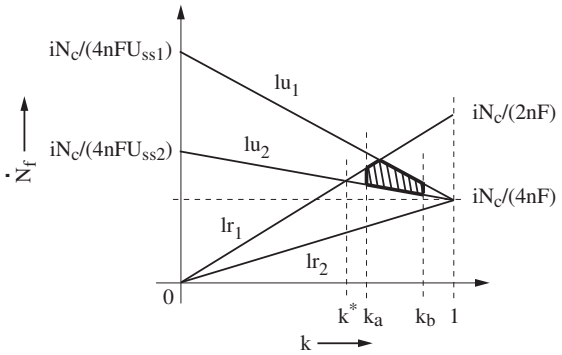

Figure 7. STEADY-STATE FUEL OPTIMIZATION

Optimum Fuel Operation

From Eqn.(36), we note that for ensuring a steam rich inlet flow into the reformer, we must have

$$\text{STCB}_{ss} \geq 0 \rightarrow \dot{N}_f \leq k\left(\frac{iN_c}{2nF}\right) \tag{37}$$

From Eqn.(29) we have

$$U_{ss} \geq 0 \rightarrow \dot{N}_f \geq k\left(\frac{iN_c}{4nF}\right) \tag{38}$$

and the constraints $0 < U_{ss1} \leq U_{ss} \leq U_{ss2} < 1$ are expressed as

$$\dot{N}_f\left(\frac{4nFU_{ss1}}{iN_c}\right) + (1 - U_{ss1})\,k \leq 1 \tag{39}$$

$$\dot{N}_f\left(\frac{4nFU_{ss2}}{iN_c}\right) + (1 - U_{ss2})\,k \geq 1 \tag{40}$$

Eqns.(37), (38), (39) and (40) are all linear in $\dot{N}_f$ and k and are denoted in Fig.7 by lr_1, lr_2, lu_1 and lu_2 respectively, along with the lines $k = k_a$ and $k = k_b$. Steady-state constrained fuel optimization for the steam reformer based SOFC system has thus been transformed to a problem in linear programming. From Fig.7 and from Eqns.(37) through (40), we can easily deduce that a solution region exists if $k_b \geq k^*$, where k^* is the value of k at the intersection between the lines lr_1 and lu_2. Hence, from Eqns.(37) and (40) we have:

$$k^* = \frac{1}{1 + U_{ss2}} \;\rightarrow\; k_b \geq \frac{1}{1 + U_{ss2}} \tag{41}$$

From Fig.7 it is also evident that if Eqn.(41) is satisfied, then the steady-state minimum fuel operating point is at the intersection

of lu_2 and $k = k_b$, given by

$$k = k_b, \quad U = U_{ss2}, \quad \dot{N}_{f,min} = \frac{iN_c}{4nFU_{ss2}} \left[1 - (1 - U_{ss2})\, k_b\right] \quad (42)$$

CONCLUSION

In this paper we investigated the transient and steady-state behaviors of utilization and steam-to-carbon balance for a reformer based SOFC system with anode recirculation and with methane as fuel. Based on a detailed control-oriented lumped model of the system, where the mass transfer and chemical kinetics phenomena of the reformer and anode control volumes were expressed in state-space form, we derived closed-form expressions that characterize these critical performance variables. Our analysis was facilitated by coordinate transformations that led to elimination of non-linear reaction rate terms from the coupled dynamic equations of the reformer and anode volumes. The estimates of time constants and steady-state values for the aforementioned performance variables matched very closely with simulations. The results were applied to address a steady-state fuel optimization problem for the SOFC system using a linear-programming based constrained optimization approach, and a minimum fuel operating point was determined. The results developed in this paper can potentially be used in a predictive manner along with sensor data to develop control strategies for SOFC based power plants.

REFERENCES

[1] Kandepu, R., Imsland, L., Foss, B. A., Stiller, C., Thorud, B., and Bolland, O., 2007. "Modeling and control of a sofc-gt-based autonomous power system". *Energy*, **32**, pp. 406–417.

[2] Mueller, F., Brouwer, J., Jabbari, F., and Samuelsen, S., 2006. "Dynamic simulation of an integrated solid oxide fuel cell system including current-based fuel flow control". *ASME Journal of Fuel Cell Science and Technology*, **3**, pp. 144–154.

[3] Xu, J., and Froment, G. F., 1989. "Methane steam reforming, methanation and water-gas shift: I. intrinsic kinetics". *AIChE Journal*, **35**(1), pp. 88–96.

[4] Achenbach, E., and Riensche, E., 1994. "Methane/steam reforming kinetics for solid oxide fuel cells". *Journal of Power Sources*, **52**, pp. 283–288.

[5] Hall, D. J., and Colclaser, R. G., 1999. "Transient modeling and simulation of a tubular solid oxide fuel cell". *IEEE Transactions on Energy Conversion*, **14**(3), pp. 749–753.

[6] Lazzaretto, A., Toffolo, A., and Zanon, F., 2004. "Parameter setting for a tubular sofc simulation model". *ASME Journal of Energy Resources Technology*, **126**, pp. 40–46.

[7] Li, P., and Chyu, M. K., 2003. "Simulation of the chemical/electrochemical reactions and heat/mass transfer for a tubular sofc in a stack". *Journal of Power Sources*, **124**, pp. 487–498.

[8] Xue, X., Tang, J., Sammes, N., and Du, Y., 2005. "Dynamic modeling of single tubular sofc combining heat/mass transfer and electrochemical reaction effects". *Journal of Power Sources*, **142**, pp. 211–222.

[9] Aguiar, P., Adjiman, C. S., and Brandon, N. P., 2005. "Anode supported intermediate-temperature direct internal reforming solid oxide fuel cell, ii. model-based dynamic performance and control". *Journal of Power Sources*, **147**, pp. 136–147.

[10] Campanari, S., and Iora, P., 2005. "Comparison of finite volume sofc models for the simulation of a planar cell geometry". *Fuel Cells*, **1**, pp. 34–51.

[11] Lu, N., Li, Q., Sun, X., and Khaleel, M. A., 2006. "The modeling of a standalone solid-oxide fuel cell auxilliary power unit". *Journal of Power Sources*, **161**, pp. 938–948.

[12] Xi, H., Sun, J., and Tsourapas, V., 2007. "A control oriented low order dynamic model for planar sofc using minimum gibbs free energy method". *Journal of Power Sources*, **165**, pp. 253–266.

[13] Achenbach, E., 1995. "Response of a solid oxide fuel cell to load change". *Journal of Power Sources*, **57**, pp. 105–109.

[14] Ferrari, M. L., Traverso, A., Magistri, L., and Massardo, A. F., 2005. "Influence of anodic recirculation transient behavior on the sofc hybrid system performance". *Journal of Power Sources*, **149**, pp. 22–32.

[15] Sedghisigarchi, K., and Feliachi, A., 2004. "Dynamic and transient analysis of power distribution systems with fuel cells - part 1: Fuel-cell dynamic model". *IEEE Transactions on Energy Conversion*, **19**(2), pp. 423–428.

[16] Mazumder, S. K., Pradhan, S. K., Acharya, K., Hartvigsen, J., von Spakovsky, M. R., and Haynes, C., 2004. "Load transient mitigation techniques for solid-oxide fuel cell (sofc) power-conditioning system". *INTELEC 2004; 26th Annual International Telecommunications Energy Conference*, pp. 174–181.

[17] Karnik, A. Y., and Sun, J., 2005. "Modeling and control of an ejector based anode recirculation system for fuel cells". *Proceedings of ASME Fuel Cell 2005*, pp. 721–731.

[18] Wark, K., 1988. *Thermodynamics*, fifth ed. McGraw-Hill, Inc., New York, NY.

[19] Incropera, F. P., and DeWitt, D. P., 2002. *Fundamentals of Heat and Mass Transfer*, fifth ed. John Wiley & Sons, Inc.

[20] Bove, R., Lunghi, P., and Sammes, N. M., 2005. "Sofc mathematic model for systems simulations - part 2: Definition of an analytical model". *International Journal of Hydrogen Energy*, **30**, pp. 189–200.